# Three-dimensional Unsteady Flow over a Heaving Rectangular Wing

K. Siva Kumar*[1], Sharanappa V. Sajjan[2]

Computational and Theoretical Fluid Dynamics Division,

Council of Scientific and Industrial Research-National Aerospace Laboratories,
Bangalore, Karnataka, India-560017

*[1]shivak@ctfd.cmmacs.ernet.in; [2]svsajjan@ctfd.cmmacs.ernet.in

***Abstract***

Three-dimensional unsteady RANS computations are performed for the flow past a pure heaving/plunging rectangular wing to study the effect of reduced frequency and heaving amplitude on the thrust generation and propulsive efficiency. The numerical solution has been obtained by using an implicit Reynolds-averaged Navier-Stokes solver IMPRANS that employs finite volume nodal point spatial discretization scheme with dual time stepping. The results are obtained in the form of aerodynamic coefficients, thrust coefficient and propulsion efficiency and compared with the available data in the literature.

***Keywords***

*Unsteady Flow; RANS Solver; Implicit Method; Dual Time Stepping; Heaving or Plunging Wing*

## Introduction

It is well known that pure "plunging" or "heaving" wing can produce both lift and thrust with certain combinations of plunging amplitude and frequency. The origin of thrust generation for an oscillating aerofoil was found by Knoller and later independently by Betz. The ability of a sinusoidally plunging aerofoil or wing can generate thrust. This effect is known as the "Knoller-Betz or Katzmayer effect". The Knoller-Betz effect was demonstrated in a wind tunnel experiment by Katzmayer. Also some experimental and computational investigation of the Knoller Betz effect was done by Jones *et al.* Following this, a number of studies for theoretical and numerical models of oscillating aerofoils were developed by Garrick and Lighthill for thin aerofoils oscillating in inviscid flow. They significantly overestimated the propulsion efficiency (Isogai et al., Ramamurti and Sandberg) observed in the low-Reynolds-number separated flows in natural flight and in the flight of Micro Air Vehicles (Jones *et al.*).

The Navier-Stokes simulations were performed by Tuncer and Platzer who have predicted more accurate flow patterns and propulsive efficiency. Neef and Hummel have computed the thrust coefficient values for aerofoils and three-dimensional high aspect ratio wings by using Euler solver. The reduced frequency is limited to about 0.1 to simulate the flow over the cruising large birds. In that work, they investigated the asymmetric thrust distribution during each period, and numerically demonstrated that the additional lift has no influence on thrust generation. Jones *et al.* have developed a flapping wing model for testing in a low speed wind-tunnel, and compared direct thrust measurements with the panel method results for several configurations.

Okamoto and Yasuda experimentally investigated aerodynamic characteristics of unsteady flow over the wings at low Reynolds number. The aerodynamic forces and moment acting on wings of aspect ratio 6 with heaving and feathering oscillations in a wind tunnel were measured at a low Reynolds number less than 104.

Jones *et al.* have investigated both experimentally and numerically for a sinusoidal flapping finite aspect-ratio wing with pure heave motion. They used a flat plate theory, two and three-dimensional panel codes, Euler and Navier-Stokes solvers for their numerical analysis. The reduced frequency, mean angle of attack, aspect ratio and Reynolds number are varied in their computations.

The present work describes the unsteady flow simulation over a rectangular wing moving with pure sinusoidal plunge motion for different combinations of plunge amplitude and reduced frequency in each case.

## IMPRANS Solver

An implicit Reynolds-averaged Navier-Stokes solver, IMPRANS developed in-house for steady and

unsteady compressible viscous flows is employed for the present simulations. It solves unsteady RANS equations in three-dimensions in a moving domain. Dual time stepping approach is used with an implicit finite volume nodal point spatial discretization scheme. Inviscid flux vectors are calculated by using the flow variables at the six neighbouring points of hexahedral volume.

The Reynolds-averaged Navier-Stokes equations for three-dimensional unsteady compressible flow in a moving domain in non-dimensional conservative form are given by

$$\frac{\partial \bar{U}}{\partial t}+\frac{\partial E}{\partial x}+\frac{\partial F}{\partial y}+\frac{\partial G}{\partial z}=0. \quad (1)$$

Here, $\bar{U}$ is the vector of conserved variables, $E$, $F$ and $G$ flux vectors, ($x$, $y$, $z$) is the Cartesian coordinate system and $t$ is the time variable.

An implicit finite volume nodal point scheme with dual time stepping approach is employed to solve the above governing equations (1). The dual time stepping consists of an implicit discretization in real time and the marching of solution in a pseudo time to steady state at each physical time step. Use of an implicit second order accurate backward difference formula for discretization in real time and Euler's implicit time differencing formula for pseudo time results in the following equation

$$\left[I+\frac{3\Delta t^*}{2\Delta t}I+\Delta t^*\left(\frac{\partial R}{\partial U}\right)^m\right]\Delta U^m=-\Delta t^*\left[R(U^m)+\frac{3U^m}{2\Delta t}-\frac{2\overline{U}^n}{\Delta t}+\frac{\overline{U}^{n-1}}{2\Delta t}\right] \quad (2)$$

Here $U^m = U(t^*) = U(m\,\Delta t^*)$ is the solution vector at pseudo time level $m$, $\Delta U^m = U^{m+1} - U^m$ is the change in $U^m$ over the time step $\Delta t^*$ and $\Delta t$ denotes the real or physical time step that is required to resolve the physical unsteadiness of the flow. The barred quantities denote the solution vectors at the previous real time levels $n$ and $n$ - 1 whereas $R$ represents the spatial operators which give rise to the flux residual after a discretization in space.

This basic equation (2) of the implicit dual time stepping technique can be solved at each real time step by employing a finite volume nodal point spatial discretization. In this approach, the flow variables are associated with each mesh point ($i$, $j$, $k$) of the grid and the centroids of the eight neighbouring hexahedron cells surrounding the nodal point are joined to form the control volume $\Omega_{ijk}$. To facilitate the finite volume formulation, the equations are written in integral form and the surface integrals are evaluated by summing up the contributions due to the flux terms over the six faces of the computational cell. Applying integral conservative equations to each control volume, linearising the changes in flux vectors using Taylor's series expansions in time, assuming locally constant transport properties, and dropping the superscript $m$ we obtain

$$\begin{aligned}&\left(I+\frac{3\Delta t^*}{2\Delta t}I\right)\Delta U_{ijk}+\frac{\Delta t^*}{\Omega_{ijk}}\sum_{m=1}^{6}\left\{\left[\left(A-\frac{\partial E_R}{\partial x}\right)\Delta U\right]_m S_{mx}\right.\\&\left.+\left[\left(B-\frac{\partial F_S}{\partial y}\right)\Delta U\right]_m S_{my}+\left[\left(C-\frac{\partial G_T}{\partial z}\right)\Delta U\right]_m S_{mz}\right\}\\&=-\frac{\Delta t^*}{\Omega_{ijk}}\left\{\sum_{m=1}^{6}\left[(E_I-E_V)_m S_{mx}+(F_I-F_V)_m S_{my}+(G_I-G_V)_m S_{mz}\right]\right\}\\&-\Delta t^*\left(\frac{3U_{ijk}}{2\Delta t}-\frac{2\overline{U}^n_{ijk}}{\Delta t}+\frac{\overline{U}^{n-1}_{ijk}}{2\Delta t}\right),\end{aligned} \quad (3)$$

Here $\Omega_{ijk}$ is the control volume surrounding the nodal point ($i$, $j$, $k$) of the curvilinear grid; $A = \partial E_I / \partial U$, $B = \partial F_I / \partial U$, $C = \partial G_I / \partial U$, $E_R = \partial E_{V1} / \partial U_x$, $F_S = \partial F_{V2} / \partial U_y$ and $G_T = \partial G_{V3} / \partial U_z$ are the Jacobian matrices; $E_I$, $F_I$ and $G_I$ are the inviscid flux vectors and $E_V$, $F_V$ and $G_V$ are the viscous flux vectors; $S_{mx}$, $S_{my}$ and $S_{mz}$ are the $x$, $y$ and $z$ components of the surface vector corresponding to the $m^{\text{th}}$ surface of the control volume.

It is important to note that the terms containing inviscid flux vectors can be calculated by using the flow variables at the six neighbouring points and Taylor's series expansions can be utilised to discretize the derivatives in the viscous flux terms directly in the physical plane. The resulting block tridiagonal system of equations is solved by using a suitable block tridiagonal solution algorithm and proper initial and boundary conditions. In order to ensure convergence and to suppress oscillations near shock waves, a blend of second and fourth order artificial dissipation terms is added explicitly. Implicit second order dissipation terms are also added to improve the practical stability bound of the implicit scheme. The algebraic eddy viscosity model due to Baldwin and Lomax is used for turbulence closure.

For a moving body, the equations are solved in the inertial frame of reference by employing a grid which remains fixed to the body and moves along with it. At each real time step $t + \Delta t$, starting from the solution at the previous time step $t$, the solution is marched in pseudo time $t^*$ using local time stepping. Since the choice of physical time step $\Delta t$ is no longer limited by stability considerations, a much larger time step, with a fixed but small number of inner iterations in pseudo time, can be used to reduce the undesirably large computational time for unsteady flow calculations. Based on this dual time stepping method an implicit Reynolds averaged Navier-Stokes solver IMPRANS

has been developed at CSIR-National Aerospace Laboratories for computing a wide variety of two-dimensional and three-dimensional unsteady viscous compressible flows. This RANS solver has been extensively validated for computing unsteady flow past pitching aerofoils and wings, plunging aerofoils, helicopter rotor blades, wind turbines etc. Here, the solver is used for three-dimensional unsteady compressible viscous flows over a pure-plunging rectangular wing.

## Results

For all the present simulations, a structured single block C-H grid around a NACA 0014 rectangular wing of aspect ratio 8 is generated using the commercial software package Gridgen V 15.5. The far-field boundary is kept at 20 chords away from the wing surface. The volume grid used for the present computations is shown in Fig. 1(a). While the surface grid on the wing is shown in Fig. 1(b). The number of grid points is 247 × 65 × 75 in the chord wise, normal and span-wise directions respectively. The points are clustered properly near the leading and trailing edges and near the tip of the wing, the first grid spacing normal to the wall being $2.0\times10^{-5}$c.

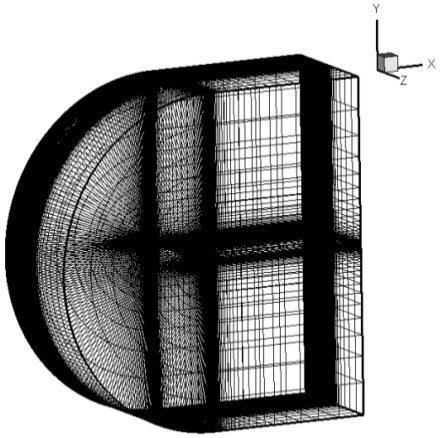


FIG. 1(a) C-H TOPOLOGY GRID AROUND THE WING

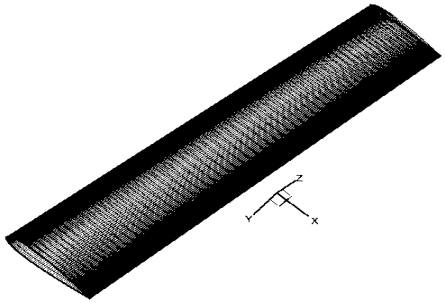


FIG. 1(b) SURFACE GRID ON THE WING

The three-dimensional unsteady flow over a pure-plunging rectangular wing has been simulated for different input parameters using implicit Reynolds averaged Navier-Stokes solver IMPRANS. The cases considered closely approximate the experimental model of Jones *et al*. Three different plunge amplitudes, $y_o$ = 0.1c, 0.2c and 0.4c with different reduced frequencies of $k$ = 0.4, 0.6, 0.8 and 1.0 are considered.

For all unsteady simulations, steady solution is first obtained. After steady state convergence is reached, the unsteady flow computation is started with a prescribed sinusoidal plunging motion. Five consecutive cycles are computed to obtain periodic solution. The final cycle results are used to calculate time averaged thrust coefficient and propulsive efficiency.

The motion of a single finite aspect ratio wing with a pure plunge motion in normal direction is defined by

$$y(t^*) = h_a \cos(k\, t^*) \quad (4)$$

and the plunging velocity is given by the following expression

$$\dot{y}(t^*) = -h_a k \sin(k\, t^*) \quad (5)$$

where non-dimensional heave amplitude, $h_a = y_o / c$, reduced frequency, $k = \omega c/U_\infty$ and non-dimesional time is $t^*$ (i.e., pseudo time).

The mean thrust coefficient and propulsion efficiency are computed using the following expressions.

The mean or time-averaged thrust coefficient is defined as

$$\overline{C}_t = -\overline{C}_d + (C_d)_{\text{steady}} \quad (6)$$

where $\overline{C}_d$ is the mean drag coefficient averaged for one period of heaving oscillation. $(C_d)_{\text{steady}}$ is the steady drag of the non-moving wing at its present angle of attack.

The % propulsion efficiency can be calculated from the ratio between power output and power input, in this case, it is given by

$$\%\ \text{Propulsion efficiency}, (\eta_{\text{prop}}) = (\overline{C}_t)/(\overline{C}_p) \quad (7)$$

where mean power input coefficient, $\overline{C}_p$ is calculated from the product of lift coefficient, $C_l$ and plunging velocity, $\dot{y}(t^*)$.

TABLE 1 AERODYNAMIC PARAMETERS USED FOR HEAVING RECTANGULAR WING

| **Input flow parameters** | |
|---|---|
| Free stream Mach Number ($M_\infty$) | 0.3 |
| Free stream Reynolds Number ($Re_\infty$) | $1.0\times10^6$ |
| Angle of attack ($\alpha$) | 2° |
| Reduced frequency ($k$) | 0.4, 0.6, 0.8 and 1.0 |
| Plunge or heave amplitude ($y_o$) | 0.1c, 0.2c and 0.4c |

The input flow parameters used for the present computations are listed in Table 1 for heaving rectangular wing.

***Case A ($h_a$ = 0.4, k = 0.4, 0.6, 0.8 and 1.0)***

In this case, the reduced frequency is varying from 0.4 to 1.0 in steps of 0.2 with the plunging amplitude of 0.4. Table 2 shows the time-averaged thrust coefficient and propulsion efficiency for the rectangular plunging wing. The propulsion efficiency values for $k$ = 0.4 and $k$ = 1.0 are compared with the available results of Jones *et al*. At the reduced frequency, $k$ = 0.4 the present computed value is 67.38% and the Jones *et al.* values are 64.15% (NS (FLOWer)), 67.29% (EULER (FLOWer)) and 68.66% (PANEL). Similarly at $k$ = 1.0 the present value is 49.73% and the Jones *et al.* values are 51.09% (NS (FLOWer)), 56.01% (EULER (FLOWer)) and 56.55% (PANEL). The present computed values are in good agreement with the results of Jones *et al*.

From the Table 2, it can be concluded that the higher thrust coefficient of 0.12864 is obtained at higher reduced frequency, while on the contrary for higher efficiency of 67.38% obtained at lower reduced frequency.

TABLE 2 COMPARISON OF MEAN-THRUST COEFFICIENT AND PROPULSION EFFICIENCY

| $k$ | $\bar{C}_t$ (Present) | % $\eta_{prop}$ (Present ) | % $\eta_{prop}$ (Jones *et al.* [11]) |
|---|---|---|---|
| 0.4 | 0.03545 | 67.38 | 64.15 (NS (FLOWer)) 67.29(EULER(FLOWer)) 68.66 (PANEL) |
| 0.6 | 0.06208 | 59.85 | - |
| 0.8 | 0.09379 | 54.65 | - |
| 1.0 | 0.12864 | 49.73 | 51.09 (NS (FLOWer)) 56.01 (EULER (FLOWer)) 56.55 (PANEL) |

The variation of lift coefficient with heave distance at different reduced frequencies is shown in Fig. 2. The lift coefficient values are higher during down-stroke than those during up-stroke. The computed loops of the aerodynamic coefficients clearly demonstrate the hysteretic property existing between the up-stroke and down-stroke in all the three cases. The variation of thrust coefficient with the heave distance at different reduced frequencies is plotted in Fig. 3. The thrust coefficient values are smaller during the first half of the down-stroke compared to the second half of up-stroke and become higher during the second half of down-stroke than those during the first half of up-stroke.

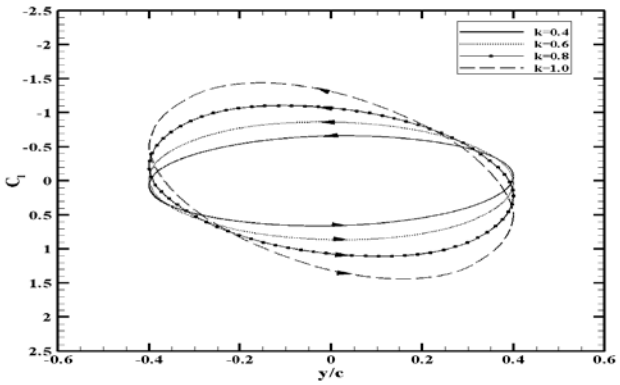


FIG. 2 THE VARIATION OF LIFT COEFFICIENT WITH HEAVE DISTANCE FOR THE HEAVING WING AT $h_a$ = 0.4

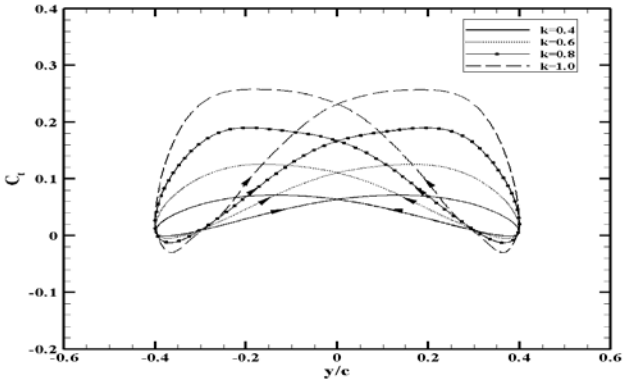


FIG. 3 THE VARIATION OF THRUST COEFFICIENT WITH HEAVE DISTANCE FOR THE HEAVING WING AT $h_a$ = 0.4

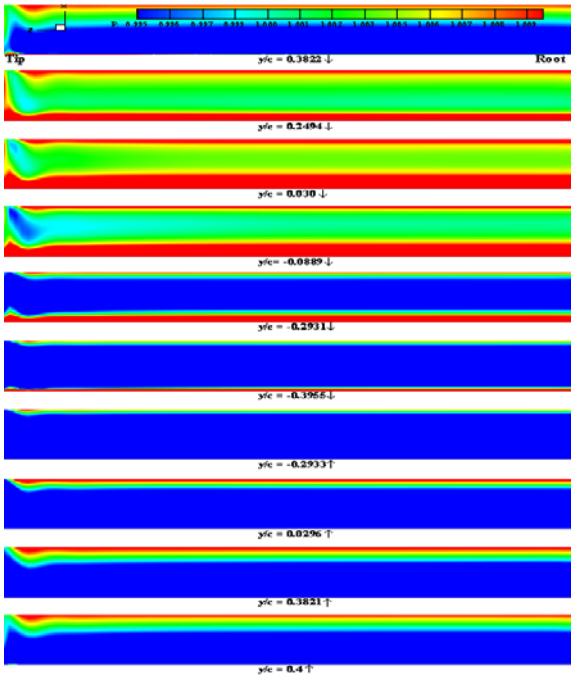


FIG. 4 SURFACE PRESSURE CONTOUR ON LOWER SURFACE OF HEAVING WING FOR ONE COMPLETE CYCLE OF OSCILLATION AT $h_a$ = 0.4 AND $k$ = 0.6

***Case B ($h_a$ = 0.1, k = 0.4, 0.6, 0.8 and 1.0)***

In this case, the reduced frequency is varying from 0.4

to 1.0 in steps of 0.2 with heaving amplitude of 0.1. Table 3 shows the time-averaged thrust coefficient and propulsion efficiency on the rectangular plunging wing for different reduced frequencies. From the results, it is observed that the higher thrust coefficient of 0.008398 is obtained at higher reduced frequency, while on the contrary for higher efficiency of 66.81% obtained at lower reduced frequency.

TABLE 3 MEAN THRUST COEFFICIENT AND PROPULSION EFFICIENCY

| $k$ | $\bar{C}_t$ | % $\eta_{prop}$ |
|---|---|---|
| 0.4 | 0.002187 | 66.81 |
| 0.6 | 0.003926 | 60.84 |
| 0.8 | 0.005989 | 57.31 |
| 1.0 | 0.008398 | 54.87 |

The variation of lift coefficient with heave distance at different reduced frequencies is shown in Fig. 5. The lift coefficient values are higher during down-stroke than those during up-stroke. The variation of thrust coefficient with the heave distance at different reduced frequencies is plotted in Fig. 6. The thrust coefficient values are smaller during the first half of down-stroke compared to the second half of up-stroke and become higher during the second half of down-stroke than those during the first half of up-stroke.

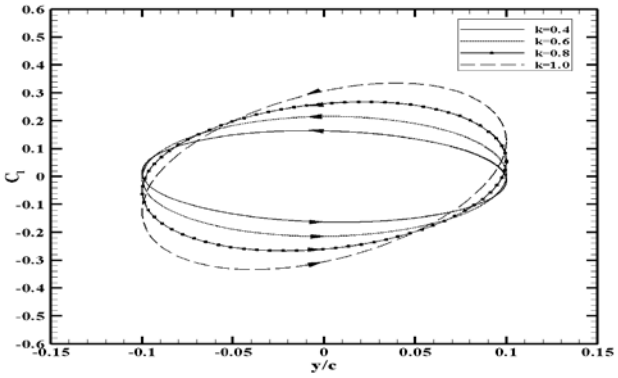


FIG. 5 THE VARIATION OF LIFT COEFFICIENT WITH HEAVE DISTANCE FOR THE HEAVING WING AT $h_a = 0.1$

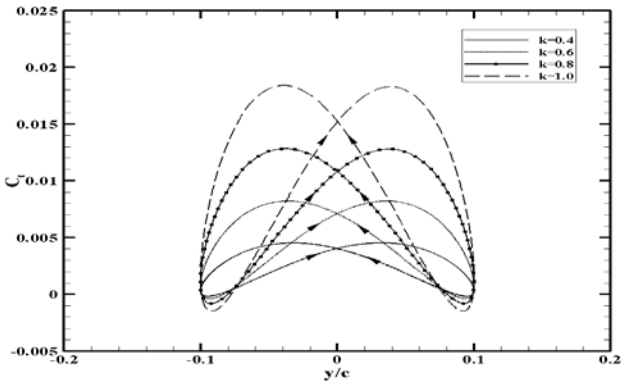


FIG. 6 THE VARIATION OF THRUST COEFFICIENT WITH HEAVE DISTANCE FOR THE HEAVING WING AT $h_a = 0.1$

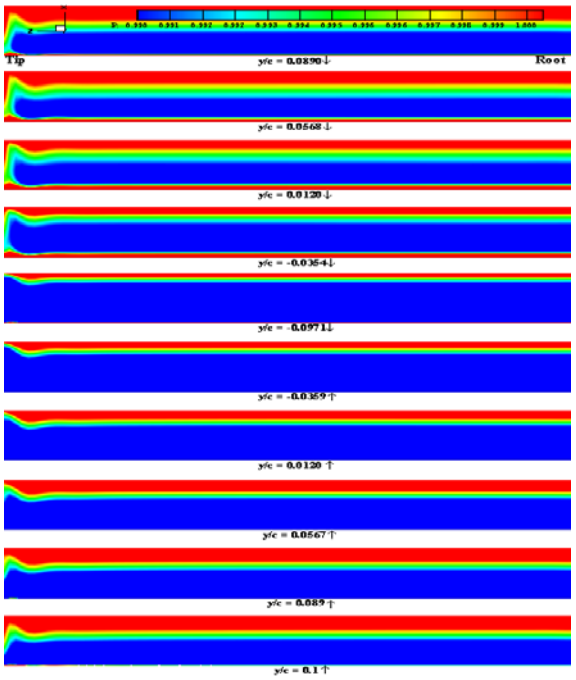


FIG. 7 SURFACE PRESSURE CONTOUR ON LOWER SURFACE OF HEAVING WING FOR ONE COMPLETE CYCLE OF OSCILLATION AT $h_a = 0.1$ AND $k = 1.0$

### *Case C ($h_a = 0.2$, $k = 0.4, 0.6, 0.8$ and $1.0$)*

In this case, the reduced frequency is varying from 0.4 to 1.0 in steps of 0.2 with the plunging amplitude of 0.2. Table 4 shows the time-averaged thrust coefficient and propulsion efficiency on the plunging rectangular wing. The higher thrust coefficient of 0.03338 is obtained at higher reduced frequency, while on the contrary for the higher efficiency of 67.57% obtained at lower reduced frequency.

TABLE 4 MEAN THRUST COEFFICIENT AND PROPULSION EFFICIENCY

| $k$ | $\bar{C}_t$ | % $\eta_{prop}$ |
|---|---|---|
| 0.4 | 0.00888 | 67.57 |
| 0.6 | 0.01575 | 60.80 |
| 0.8 | 0.02374 | 56.42 |
| 1.0 | 0.03338 | 53.70 |

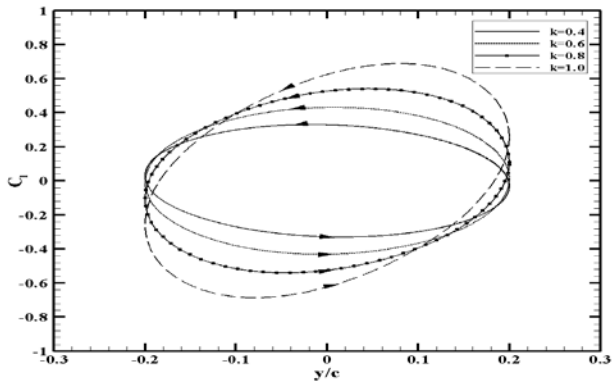


FIG. 8 THE VARIATION OF LIFT COEFFICIENT WITH HEAVE DISTANCE FOR THE HEAVING WING AT $h_a = 0.2$

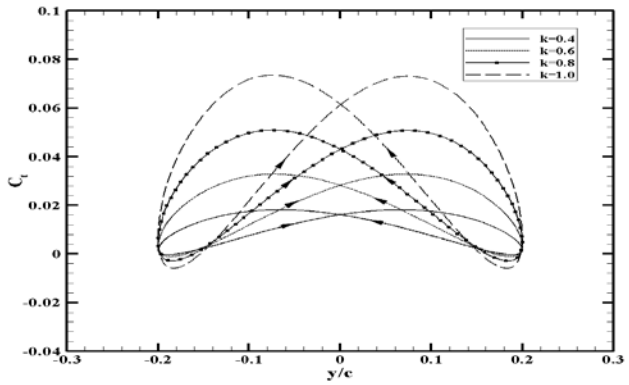


FIG. 9 THE VARIATION OF THRUST COEFFICIENT WITH HEAVE DISTANCE FOR THE HEAVING WING AT $h_a$ = 0.2

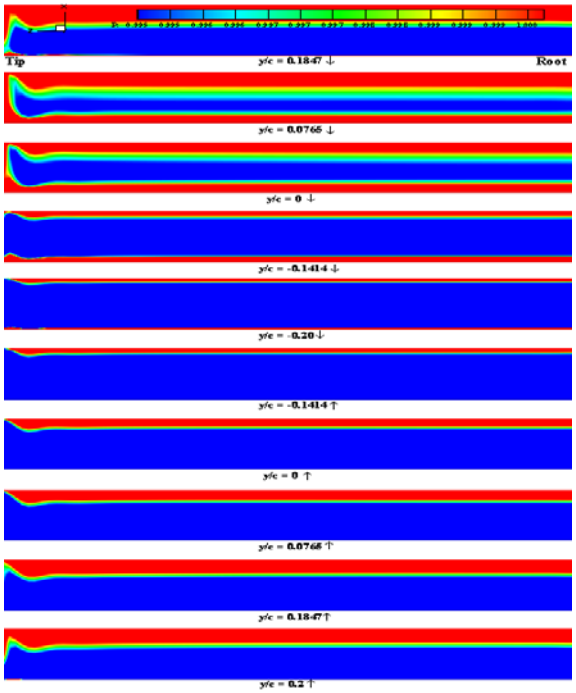


FIG. 10 SURFACE PRESSURE CONTOUR ON LOWER SURFACE OF HEAVING WING FOR ONE COMPLETE CYCLE OF OSCILLATION AT $h_a$ = 0.2 AND $k$ = 0.8

The unsteady variation of lift coefficient with heave distance at different reduced frequencies is shown in Fig. 8. The lift coefficient values are higher during down-stroke than those during up-stroke. The results plotted in Fig. 9 show the unsteady variations of thrust coefficient with the heave distance at different reduced frequencies. The thrust coefficient values are smaller during the first half of down-stroke compared to the second half of up-stroke and become higher during the second half of down-stroke than those during the first half of up-stroke.

For all the three cases, the surface pressure fields are plotted in Figs. 4, 7 and 10 on the lower surface of the heaving rectangular wing for one complete cycle with non-dimensional heave amplitudes of 0.4, 0.1 and 0.2 at $k$ = 0.6, 1.0 and 0.8 respectively. From the all surface pressure plots, it is observed that near the tip of the wing initially more variations have been observed at the beginning of the cycle (i.e., downward stroke) than those at the middle and again more variations at the end of the cycle (i.e., upward stroke).

The comparison of mean thrust coefficient and propulsion efficiency at different heave amplitude '$h_a$' values are shown in Figs. 11 and 12 respectively, for the heaving wing. As '$k$' or '$h_a$' increases, the time-averaged thrust coefficient increases and propulsion efficiency decreases for the range considered.

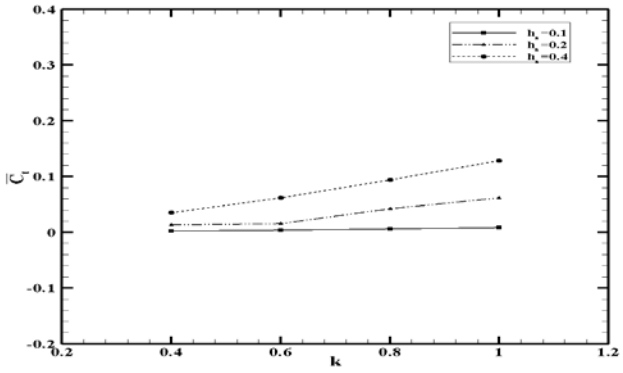


FIG. 11 THE COMPARISON OF MEAN THRUST COEFFICIENT AT DIFFERENT NON-DIMENSIONAL HEAVE AMPLITUDE '$h_a$' VALUES FOR THE HEAVING WING

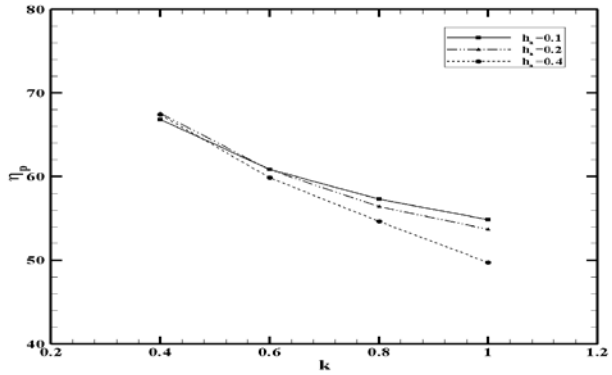


FIG. 12 THE COMPARISON OF PROPULSION EFFICEINCY AT DIFFERENT NON-DIMENSIONAL HEAVE AMPLITUDE '$h_a$' VALUES FOR THE HEAVING WING

## Conclusions

The unsteady flow over a rectangular heaving wing has been computed by using implicit Reynolds averaged Navier-Stokes solver IMPRANS. The effect of heaving amplitude and reduced frequency on the propulsive efficiency and time-averaged thrust coefficient has been studied. The computed results agree well with the available data in the literature. From the results, it is observed that as reduced frequency increases, the time-averaged thrust coefficient increases and propulsion efficiency

decreases for the range of values considered in the present computations. In all the cases, higher thrust occurred at higher reduced frequency, while higher propulsive efficiency occurred at lower reduced frequency. The higher thrust coefficient of 0.12864 is obtained at higher reduced frequency of 1.0, while on the contrary for higher efficiency of 67.38% obtained at lower reduced frequency of 0.4 at the heaving amplitude of $h_a$ = 0.4 and the higher thrust coefficient of 0.008398 is obtained at higher reduced frequency of 1.0, while for higher efficiency of 66.81% at lower reduced frequency of 0.4 the heaving amplitude of $h_a$ = 0.1. And the higher thrust coefficient of 0.03338 is obtained at higher reduced frequency of 1.0, while higher efficiency of 67.57% at lower reduced frequency of 0.4 the heaving amplitude of $h_a$ = 0.2. As heave amplitude, $h_a$ increases, the time-averaged thrust coefficient increases and propulsion efficiency decreases for the range considered in the present work.

## ACKNOWLEDGMENT

The authors gratefully acknowledge Dr. P. K. Dutta for his constant encouragement and support during the work.

## REFERENCES

Baldwin, B. S. and Lomax, H., "Thin Layer Appro-ximation and Algebraic Model for Separated Turbulent Flows", AIAA Paper No. 78 - 257, 1978.

Beam, R. M. and Warming, R.F, "An Implicit Finite Difference Algorithm for Hyperbolic Systems in Conservation-Law Form", Volume 22, Issue 1, PP. 87–110, September 1976.

Dutta, P. K., Vimala Dutta and Sharanappa, "An Implicit RANS Solver for Unsteady Compressible Flow Computations", Proc. Seminar on State of the Art and Future Trends of CFD at NAL, NAL SP 0301, NAL, Bangalore, 2003.

Dutta, P. K., Vimala Dutta and Sharanappa, "RANS Computation of Flow past Wind Turbine Blades", Proc. 7th Asian Computational Fluid Dynamics Conference (ACFD7), Bangalore, November 26th - 30th , Paper 8.1, pp. 335 - 353, 2007.

Garrick, I. E., "Propulsion of a Flapping and Oscillating Airfoil", NACA Report 567, 1936.

Isogai, K., Shinmoto, Y. and Watanabe, Y., "Effects of Dynamic Stall on Propulsive Efficiency and Thrust of Flapping Airfoil", AIAA Journal, Vol. 37, pp. 1145 - 1151, October 1999.

Jones, K. D., Dohring, C. M and Platzer, M. F., "Experimental and Computational Investigation of the Knoller Betz Effect" AIAA Journal, Vol. 36, No. 7, pp. 1240 - 1246, July 1998.

Jones, K. D., Duggan, S. J. and Platzer, M. F., "Flapping-wing propulsion for a micro air vehicle", AIAA Paper 2001 - 0126, 39th Aerospace Sciences Meeting & Exhibit, 2001.

Jones, K. D., Platzer, M. F. and Lund, T. C., "Experi-mental and Computational Investigation of Flapping-Wing Propulsion for Micro Air Vehicles", Chapter 16, Fixed and Flapping Wing Aerodynamics for Micro Air Vehicle Applications, Mueller, T. J. (ed.), Progress in Astronautics and Aeronautics Series, AIAA, Reston VA, pp. 307 - 339, 2001.

Jones, K. D., Castro, B. M., Mahmoud, O., Pollard, S. J. and Platzer, M. F., "A Collaborative Numerical and Experimental investigation of flapping wing propulsion", AIAA Paper No. 2002 - 0706, January 2002.

Lighthill, M. J., "Aquatic Animal Propulsion of High Hydro-mechanical Efficiency", J. Fluid Mech., Vol. 44, No. 2, pp. 265 - 301, 1970.

Neef, M. F. and Hummel, D., "Euler solutions for a finite-span flapping wing", Tech. rep., Conference on fixed, flapping and rotary wing vehicles at very low Reynolds numbers, University of Norte Dame, Indina, June 2000.

Okamoto, M. and Yasuda, K., "Experimental Study on Aerodynamic Characteristics of Unsteady Wings at Low Reynolds Number", AIAA Journal, Vol. 43, No. 12, 2005.

Pulliam, T. H., "Implicit Solution Methods in Computational Fluid Dynamics", App. Num. Math., (Trans. IMACS), 2, 6, pp. 441 - 474, 1986.

Ramamurti, R. and Sandberg, W., "Simulation of Flow about Flapping Airfoils using Finite Element Incompressible Flow Solver", AIAA Journal, Vol. 39, pp. 253 - 260, 2001.

Sharanappa, Vimala Dutta and Dutta, P. K., "Viscous Unsteady Flow around a Helicopter Rotor Blade in Forward Flight". Proc. 9th Annual CFD Symposium, CFD Division of Aeronautical Society of India, Bangalore, August 11th - 12th , CP13, 2006.

Sharanappa V. Sajjan, Vimala Dutta and Dutta, P. K., "Numerical Simulation of flow over pitching bodies

using an implicit Reynolds-averaged Navier-Stokes solver", Proc. of 12th Asian congress of Fluid Mechanics, Daejeon, Korea, August 18th - 21st, 2008.

Siva Kumar, K. and Sharanappa V. Sajjan, "Compu-tation of Unsteady Flow over a Plunging Aerofoil Using an Implicit Reynolds averaged Navier-Stokes Solver", Proc. of 8th Asian Computational Fluid Dynamics Conference (ACFD8), Hong Kong, January10th - 14th, 2010.

Tuncer, I. H. and Platzer, M. F., "Thrust Generation due to Airfoil Flapping", AIAA Journal, Vol. 34, No. 2, pp. 324 - 331, 1996.

Vimala Dutta, Sharanappa and Dutta, P. K., "Navier-Stokes Computations for a Helicopter Rotor Blade in Hover", Proc. 8th Annual CFD Symposium, CFD Division of Aeronautical Society of India, Bangalore, August 11th - 13th, CP 18, 2005.